# Nanopages

## Optical properties of bioinspired disordered photonic nanoarchitectures

--Manuscript Draft--

| | |
|---|---|
| **Manuscript Number:** | |
| **Full Title:** | Optical properties of bioinspired disordered photonic nanoarchitectures |
| **Article Type:** | Original Research Paper |
| **Section/Category:** | Basic Science Section |
| **Keywords:** | bioinspired; structural color; disordered; nanospheres; diffuse reflection; light coupling |
| **Corresponding Author:** | István Tamáska<br>HUNGARY |
| **Corresponding Author Secondary Information:** | |
| **Corresponding Author's Institution:** | |
| **Corresponding Author's Secondary Institution:** | |
| **First Author:** | István Tamáska |
| **First Author Secondary Information:** | |
| **Order of Authors:** | István Tamáska |
| | Zofia Vértesy, Ph.D. |
| | András Deák, Ph.D. |
| | Péter Petrik, Ph.D. |
| | Krisztián Kertész, Ph.D. |
| | László Péter Biró, D.Sc. |
| **Order of Authors Secondary Information:** | |
| **Abstract:** | Bioinspired 1+2D nanoarchitectures inspired by the quasi-ordered structures occurring in photonic nanoarchitectures of biological origin, like for example butterfly scales, were produced by depositing a layer of SiO2 nanospheres (156 nm and 292 nm in diameter) on Si wafers, over which a regular multilayer composed from three alternating layers of SiO2 and TiO2 was deposited by physical vapor deposition. Flat multilayers were deposited in the same run on oxidized Si (324 nm SiO2 thickness) for comparison. Different types of disorder (in plane and out of plane) were purposefully allowed in the 1+2D nanoarchitectures. The positions of the specular reflection maxima for the flat multilayer and for the two different bioispired nanoarchitectures were found to be similar. Additionally to this, the bioinspired nanoarchitectures exhibited angle independent diffuse reflection too, which was absent in the flat multilayer. Different model calculations were made to explain the specular and diffuse optical properties of the samples. Satisfactory agreement was obtained between experimental results data and model calculations. |
| **Suggested Reviewers:** | Olivier Deparis, Prof.<br>Université De Namur<br>olivier.deparis@unamur.be |
| | Zsuzsanna Rajkovits, Ph.D.<br>Eötvös Loránd University<br>rajzsu@ludens.elte.hu |
| **Opposed Reviewers:** | |

# Optical properties of bioinspired disordered photonic nanoarchitectures

István Tamáska[a], Zofia Vértesy[a], András Deák[a], Péter Petrik[a], Krisztián Kertész[a] and László P. Biró[a,*]

*[a]Research Centre for Natural Sciences, Institute of Technical Physics and Materials Science, P.O. Box 49, H-1525 Budapest, Hungary (http://www.nanotechnology.hu/)*

** Corresponding author: Prof. László Péter Biró. E-mail: biro.laszlo@ttk.mta.hu, Tel:06-1-3922681*

## Abstract

Bioinspired 1+2D nanoarchitectures inspired by the quasi-ordered structures occurring in photonic nanoarchitectures of biological origin, like for example butterfly scales, were produced by depositing a layer of $SiO_2$ nanospheres (156 nm and 292 nm in diameter) on Si wafers, over which a regular multilayer composed from three alternating layers of $SiO_2$ and $TiO_2$ was deposited by physical vapor deposition. Flat multilayers were deposited in the same run on oxidized Si (324 nm $SiO_2$ thickness) for comparison. Different types of disorder (in plane and out of plane) were purposefully allowed in the 1+2D nanoarchitectures. The positions of the specular reflection maxima for the flat multilayer and for the two different bioinspired nanoarchitectures were found to be similar. Additionally to this, the bioinspired nanoarchitectures exhibited angle independent diffuse reflection too, which was absent in the flat multilayer. Different model calculations were made to explain the specular and diffuse optical properties of the samples. Satisfactory agreement was obtained between experimental data and model calculations.

**Keywords:** bioinspired; structural color; disordered; nanospheres; diffuse reflection; light coupling

## 1. Introduction

Photonic crystals are a particular case of nanocomposites. Taking the concept of photonic crystals in a strict sense,[1] due to the rigorously periodic alternation of the refractive index from high to low values in a three dimensional (3D) structure, and provided that the high/low contrast has a high enough value, in certain wavelength regions, called the stop-gaps, the nanocomposite will not allow the propagation of the electromagnetic waves (EMW).[1] Later on, the concept was significantly extended to include metallic photonic nanoarchitectures[2] and partially[3-5] or fully disordered systems too.[6,7] Nowadays, photonic crystals are regarded as particular case of the broader category of metamaterials.[8] There is a growing interest to the field of photonic crystals that comes from the ability of the photonic crystals to manipulate and control light propagation in three dimensions in space. On the other hand, the manufacturing of defect free large area 3D photonic crystals is still a technological challenge.[9]

Interestingly enough, biological evolution, also "discovered" the photonic nanoarchitectures as a very versatile way of producing color.[10,11] Most frequently, the photonic nanoarchitectures of biologic origin are characterized by a certain degree of disorder, which may affect their optical properties significantly.[12] It was shown recently for nine closely related butterfly species that the structural color is generated by well-defined characteristic, quasi-ordered structures, with a well-defined species specific color, which is used as a sexual recognition signal.[13] Due to this, the very same color originating from quasi-ordered photonic nanoarchitectures is reproduced with a great degree of fidelity generation by generation.

The knowledge, extracted from the investigation of biological, partially or fully disordered photonic nanoarchitectures, could provide photonic structures with structurally more robust and with more versatile optical properties than artificial opals for example. In the same time, the manufacturing of such nanocomposites could be a lot less demanding than the production of fully ordered 3D nanoarchitectures. There is a growing interest to artificially made quasi-ordered structures,[14] similar to the ones found in nature and gone through several million years of evolution. This may lead to new manufacturing procedures and may help in the discovery of new bioinspired structures. The purpose is not to copy the structures exactly which is difficult technologically and could be very expensive, rather to learn and understand the principles of biological structures and use them to fabricate photonic structures with novel properties. We used this approach in this paper.

In the present paper we made photonic nanoarchitectures in which a certain degree of disorder has been introduced purposefully. Similar nanoarchitectures have been prepared earlier, but the role of disorder and how the disordered structures may interact with light were given less consideration.[15,16] We investigated the optical and structural properties in detail, and we propose several models to understand in which ways the basic geometry and the disorder of the nanoarchitectures interact with light.

## 2. Materials end methods

The photonic nanoarchitectures modeling the butterfly scales with a certain degree of disorder were produced in several steps. First, the silica particles were prepared according to Stöber's method using tetraethyl orthosilicate (TEOS), absolute ethanol and ammonium hydroxide.[17] Different amounts of ammonium hydroxide were used to prepare silica particles of two different diameters (156 nm, 292 nm). 3 inch silicon wafers covered with native oxide were used as substrates for the deposition of the nanoparticles. For the single layer deposition, a Langmuir-Blodgett trough was used.[18] As it was not our aim to produce fully ordered layers, no special care was taken to precisely compact the dispersed nanospheres on water surface before the substrate was vertically educed from water. Fully ordered or fully disordered samples can be produced under well-defined conditions, while the conditions under which partially ordered, or quasi-ordered samples can be produced - like those occurring in butterfly wings[11,12] - are less well defined.

In a subsequent step the nanoparticles were anchored to the surface by the conformal growth of a 5 nm thick alumina layer by atomic layer deposition (ALD) method.[19,20] The ALD process was carried out using a Picosun Sunale R-series ALD reactor at 300°C with trimethylaluminium precursor and water. This anchoring process was necessary because in the previous experiments when thin films were deposited by Physical Vapor Deposition (PVD) onto the monolayer of nanospheres, the growing film caused the degradation of the nanosphere film continuity and the exfoliation of the layer. After ALD, the samples were characterized by atomic force microscopy (AFM).

In the next step 3 pairs of alternating $TiO_2/SiO_2$ layers, each with 65 nm thickness, were evaporated onto the sample by PVD. $TiO_2$ and $SiO_2$ were used as high and low refractive index materials, respectively, without significant absorption coefficient in the visible spectrum, to minimize the absorption within the multilayer. In parallel with the nanosphere layers, bare microscope slides and silicon wafers covered with native oxide and with 324 nm thermal oxide were also subjected to PVD to be used as reference samples.

After the full deposition cycle was completed the samples were characterized again by AFM and SEM. Optical characterization of the flat multilayers was done by spectral ellipsometry and in a spectrogoniometric setup using an Avantes 2048 fiber-optic spectrometer.[3] In the spectrogoniometric setup, the samples were illuminated perpendicular (0°) to the sample surface, and the reflectance was measured from 10° to 80° with 5° resolution. Ellipsometric measurements were done on a multilayer coated glass and silicon wafer substrates without nanospheres to precisely determine the thicknesses and refractive indexes of the deposited layers. The measurements were performed by a Woollam M-2000DI rotating compensator ellipsometer in the spectral range of 190-1700 nm. It showed that the thicknesses of the layers, counted from the substrate were very close to the preset value (65 nm): 64.7 nm, 61.7 nm, 67.7 nm, 62.3 nm, 66.6 nm, 67.1 nm.

## 3. Computational details

As the above described photonic nanoarchitectures are composed from nanostructures with 1D and 2D periodicity, their properties could be discussed separately with different models. The optical properties of a 1D multilayer can be modeled by transfer matrix method. In our model we used an ideal plane parallel multilayer (without interface roughness and with invariant thicknesses). This simple multilayer model contains 9 layers on top of a silicon substrate, counted from the substrate: native oxide, 156 or 292 nm $SiO_2$ depending on the diameter of the spheres, 5 nm $Al_2O_3$ and 3 pairs alternating $TiO_2$ and $SiO_2$ layers. In our models, we used the thicknesses that were measured experimentally by ellipsometry on the flat reference samples.

The effect of the 2D periodicity can be modeled by 3D numerical calculations and was performed using the MEEP implementation of the finite-difference time-domain (FDTD) method.[21] Our model systems were built up using the experimentally measured data, the cross section of the geometry can be seen in Fig 1. The native oxide layer and the alumina layer were neglected, since the thickness of these layers is much less, or comparable with the spatial resolution, and we tried to use the simplest model in order to separate the different effects. At two parallel sides of the simulation box that are perpendicular to the sample surface, Bloch periodic boundary conditions were set to make possible the reduction of the size of the computational cell (perpendicular to the cross section that can be seen on Fig. 1.). On the other sides, perfectly matched layer (PML) absorbing boundary conditions were set. The structure was excited by a Gaussian planewave source with a wide wavelength domain (200 - 1000 nm). The electric field of the source was polarized in two reciprocally perpendicular directions in a plane, parallel to the sample surface to take into account the unpolarized light source used in the experiments. For calculating the specular reflection flux ($F_{refl}$), the detector plane was placed parallel and slightly below the source plane. The intensity of the incoupled light was calculated on the detection plane placed into the multilayer ($F_{layer}$). In order to get the reference incident flux, we performed a simulation without the model photonic nanoarchitecture and measured the flux below the source plane ($F_{refl}$ plane on Fig. 1. without the geometry).

## 4. Experimental results

### *4.1 Structural investigation*

Atomic Force Microscope (AFM) measurements were done on the silica nanosphere monolayers, deposited by Langmuir-Blodgett method and stabilized by ALD deposited alumina layer. The two layers showed quite different morphology (Fig. 2.).

The layer built of smaller spheres had monolayer domains with crystalline order. It also had an out-plane disorder: many creased islands could be found in the layer, forming a second layer on the top of the first layer. The creased islands were found to be only a few 100 nm distances from each other. The average sphere distance (156±7 nm) was calculated from several line cuts not running through the creased islands, assuming closed packing.

The layer built of larger spheres showed only a short range order. This type of in-plane disorder or quasi-ordered structure can be found in the scales of butterflies and can be characterized by Fast Fourier Transformation (FFT).[12,22] A similar method can be used in this case to determine the average distance of the spheres and to characterize the disorder of the layer. With this method the diameter of the spheres cannot be determined exactly, since the FFT power spectrum contains only the structural information parallel to the surface, in other words the distance of the neighboring spheres. The FFT power spectrum calculated from the AFM image, showed a ring-like feature around the origin (Fig. 2f.). This means that the spheres are arranged randomly but have a characteristic distance from each other. On the radial average of the power spectrum (Fig. 2e.) a clear peak can be seen according to the ring on the FFT image. The position of the peak can be calculated by fitting a Gaussian, the average distance of the spheres was 292±12 nm. The real sphere diameter may be somewhat smaller, because it is hard to measure precisely the average diameter of the spheres with AFM when the spheres are not arranged in a closed packing, so the diameter was satisfactorily approximated with the distance of the neighboring spheres. The disorder of the samples can also be seen after the $TiO_2/SiO_2$ multilayer deposition on Fig. 3.

### *4.2 Specular reflectance*

Multilayers should have only mirror-like (specular) reflection. Since these samples are basically multilayers with two dimensional quasi-periodic roughness, it is worth to investigate the specular reflection and compare it to conventional plane multilayers.

Comparing the experimental data of the simple multilayer reference and the nanoarchitectures (Fig. 4.), when illuminated and measured perpendicular to the sample surface, one may remark a clear difference in the intensities of the reflectance maxima. The measured reflectance values on the nanostructured samples were about half of the corresponding values of the flat multilayer reference sample (Fig. 4.). This finding is not surprising if the roughness of the samples, caused by the sphere layers, is taken into account. One of the main effects expected from the irregularities in the sample structure is the appearance of scattered light. Furthermore, the size of the nanospheres did not have a marked influence on the intensity of the reflection peaks, this means that the same mechanism was responsible for the reflection of the two samples with nanospheres.

### *4.3 Diffuse reflectance*

Diffuse (Lambertian) reflection cannot be observed on conventional multilayers, since these structures have only mirror-like reflection. While on the layered structures discussed in this paper, a noticeable diffuse reflection was found. When illuminated under perpendicular incidence to the surface with white light, as compared with the specular samples, both nanoarchitectures built with the smaller and the larger nanospheres reflect light with higher intensity into all directions in the wavelength range of 400-500 nm (Fig. 5.). This is reason of the clearly seen blue color of the nanoarchitectures opposite to the black of the regular multilayer. This similar behavior should be caused by similarities in the structure of the samples. The only similarity in the samples is the $TiO_2/SiO_2$ multilayer, evaporated onto the sphere layers. Therefore it could be presumed that the nanospheres and the undulated multilayer are responsible for the diffuse reflected wavelength range.

If comparing the two nanoarchitectures with each other, one may remark a much stronger angle dependence of the reflected light intensity in the case of the smaller spheres, while the sample with the larger spheres exhibits a plateau in the range of $30^o$ to $60^o$.

One may remark from Fig. 5. c-f. that the corrugated sample with the smaller nanospheres exhibits a stronger color dependence of the reflected diffuse light with the angle of observation as compared with the sample with larger nanospheres. The later ones appear blue over the entire angular range; this corresponds to the plateau seen in Fig. 5b. The naked eye observation and the spectrogoniometric data are fully in agreement. This is a clear proof that such structures are suitable to produce an angle independent structural color in a similar way like the scales of Lyceanid butterflies.[13]

## 5. Discussion

### 5.1. Specular reflection

To be able to explain the specular reflection, the different properties of the samples have to be separated. We have seen that the specular reflection of reference sample and the samples with nanospheres have been similarly composed of several peaks. We suppose that this similarity is caused by the multilayer structure of every sample. This could be investigated by simple 1D calculation, where the 2D structure of the samples parallel to sample surface is not taken into account. The 1D model gave a very close specular reflection to the measured ones; the only discrepancy is the intensity difference (Fig. 6.). Therefore we can conclude that mainly the 1D multilayer structure is responsible for the position of the reflection peaks.

The 2D structure of the samples could be taken into account with a more complex 3D model. In these calculations we used perfectly ordered 3D FDTD structures with closed packed triangular lattice, this allows us to separate the effect of the disorder in the samples. Although the 3D FDTD model uses only constant refractive indexes, it gives better coincidence between the computed and the measured spectra. The refractive indices were chosen at the wavelength of 530 nm, because our model not allowed to use wavelength dependent refractive indices. The refraction index of the $SiO_2$ and $TiO_2$ varies more for smaller wavelengths, what means that the constant refractive index approximation gave larger discrepancy. A more refined model could be used by building the whole reflectance spectrum from several calculations which use different values of refractive indexes for different spectral ranges (Table 1.). In this model, we used the refractive indexes of the materials at the wavelength of the measured reflectance maxima, and this model also gave better fit to the experimental results in the smaller wavelength range.

The 1D models used for the two different samples predicted about twice as high reflectance maxima than the measured ones in the wavelength range of 500 - 600 nm. On the other hand the FDTD calculations predicted the correct intensities. This means that the roughness and the 3D structure of the samples caused the experimentally found lower intensities, as compared to the flat multilayers.

In the FDTD model calculations we used a perfectly ordered 3D FDTD structure. As no characteristic differences can be found between the specular reflectance measurements and the calculations, we can conclude that the disorder of the samples has only a minor effect on the specular reflection.

*5.2. Diffuse reflecion*

3D FDTD calculations in contrast with the 1D calculation are capable of better explaining how light interacts with the structure. The calculations showed that a large part of the incoming light penetrated to the multilayer, and propagated parallel to the sample surface, even a small out scattering of this propagating mode could be seen (Fig. 7.). This propagating mode could be a good explanation of the diffuse reflection properties.

Unfortunately, direct comparison between the measurements and the calculations cannot be made, since the light intensity within the multilayer cannot be measured or the intensity of the scattered light in the far field cannot be calculated in the currently used model. In order to compare quantitatively the measured light scattered under non-specular angles with the calculations, the following procedure was used: the sample was illuminated under normal incidence (0 °), and light scattered under different angles was collected using the spectrogoniometric setup. To use a simple 2D presentation of the essentially 3D experimental data and to be able to compare in a simple way the two samples with nanoarchitectures, all acquired spectra were averaged over the detecting angle. For each individual curve used in the averaging the same white diffuse standard was used as a comparison sample.

In the calculations, the spectrum of the incoupled light was measured within the multilayer (Fig. 1., on an $F_{layer}$ plane close to the source), then the intensity was doubled to take into account the light that propagates to the opposite direction ($F_{calculated}$ on Fig. 8.). In these models the refractive index of the materials were set to the values corresponding to 430 nm, where the measured diffuse peaks with the highest amplitude are found. For the larger nanospheres, the calculations showed a similar reflection peak as the measurements and give a very good agreement with the measured curves (Fig. 8.). It can be also seen that a large amount (approx. 70%) of the incoming light incouple into the multilayer.

This good agreement also means that the in-plane disorder does not affect the reflection properties of the samples too much, because perfectly ordered closed packed ordering were used in our calculations in contrast to the disorder of the measured samples. On the other hand the clearer understanding of how this in-plane disorder affects the reflection needs more extended models (supercells) where the quasi-ordered structure can be modeled in more detail. For the smaller spheres, our FDTD model cannot reproduce the reflectance spectrum. We will discuss this in detail later.

In the calculations, we have seen that a large amount of the incoming light incoupled to the multilayer with a spectrum very close to the measured ones. We could then conclude that the diffuse reflection could be modeled by the out scattering of this propagating mode, as it can be seen on Fig. 7. We have made another calculation with a longer cell, where the fluxes were measured in the multilayer on several positions ($F_{\mathrm{layer}}$ on Fig. 1. with different horizontal positions). It showed that the intensity of the reflection peak decreased with the distance from the source, what can be explained by the out scattering of light (Fig. 9.).

### *5.3. Role of the structural disorder in the optical properties*

On the model sample with the smaller spheres, we have seen that the calculated spectrum did not match with the experimental diffuse reflection. We assume that the multilayer structure has a nearly flat surface and light cannot incouple into it. As the size of the nanospheres is far from the wavelength of the illuminating light the in-plane nanostructure of the layers has less effect. It was shown by the AFM and SEM measurements that in the experiments there are creased islands where the evaporated multilayer are rougher. These surface irregularities may cause that light can more easily be incoupled into propagating modes in the structure.

To test this hypothesis, different 3D geometries were used in model calculations. Four geometries were created; each of them had one sphere under the radiation source plane which was raised slightly above the sphere layer. The cross sections of the geometries can be seen in Fig. 10. The blue area represents the region below the radiation source plane. By these small modifications, a 5 to 10 times intensity increase in the wavelength range of 350-550 nm can be achieved and correlated with the measured diffuse reflectance. The calculations also showed that the effectiveness of this coupling also depends on the vertical and horizontal position of the raised sphere. On the other hand, several calculations need to be done with different possible geometries of the creased island to achieve better fit to the measurements.

It is worth to observe that the two different kinds of disorder yield different behavior. The calculations on an ordered model with the larger spheres adequately reproduced the measured reflection curves. This shows that the in-plane disorder of the samples had less influence on the diffuse reflection spectra. On the other hand, the influence of the out of plane disorder on an in-plane ordered structure to the diffuse reflection, in the case of samples with smaller spheres, was satisfactorily reproduced by raising a sphere from the monolayer in the FDTD calculations.

## 6. Conclusions

We have created two kinds of 1+2D layered nanoarchitectures without perfect crystalline order using a 1D multilayer on top of 2D nanosphere layers. Such structures can be regarded as simplified models of nanostructures occurring in natural photonic nanoarchitectures, like butterfly wing scales. The two nanosphere layers had quite different structure. The sample with smaller nanospheres had a more ordered in-plane structure, but was exhibiting creased islands (out of plane disorder). The sample with larger nanospheres had a stronger in-plane disordered structure exhibiting only short range order. The disorder was characterized by Fourier Transformation.

Detailed spectroscopic measurements revealed that the 1+2D nanoarchitectures behave as intermediates between a simple 1D multilayer and a Lambertian reflector. They exhibited similar reflectance maxima in specular geometry as a regular, flat multilayer, but also exhibited a nonspecular component in the reflected light under any other angle of observation. This nonspecular, diffuse component is similar to the behavior of photonic nanoarchitectures with disordered nanostructures found in nature.[23] Several models were done to understand and interpret the optical properties of the samples.

Simple multilayer model showed that the reflection peaks in the specular reflectance spectra of the nanoarchitectures came from the multilayered structure of the samples. On the other hand, more complex 3D FDTD models showed that the decreased intensity of the reflection peaks came from the roughness of the multilayer, caused by the sphere layer. The in-plane disorder of the samples however seemed that did not have marked influence to the specular reflection.

The 1 + 2D nanoarchitectures exhibited diffuse reflection in the entire spectral range. Both structures had a characteristic simple peak or a double peak around the 430 nm. Detailed 3D calculations showed that after light was incoupled into the nanoarchitecture, it propagated in the undulated multilayer in a direction parallel to the sample surface. The experimentally measured peaks come from the out-scattering of this light coupled into a propagating mode in the multilayer, because of the roughness of the multilayer and probably due to the defects. The characteristic wavelength for which propagation in the plane of the multilayer is observed is determined by the structural properties of the multilayer, which can be regarded as a wavelength selective coupler.

Simulations showed that a large amount of the incoming light with this characteristic wavelength continues to propagate in the multilayer. It was also shown that a small out of plane modifications in the smaller sphere layer - as the creased islands were modeled - can drastically increase the intensity of the light incoupled into propagating modes. In the 3D models we used a perfectly ordered lattice of the spheres. However, the experimental samples showed that the layer of larger spheres had only short range order, the measured specular and diffuse reflection of the sample could be well interpreted by the calculations and no characteristic effect was found on the reflection of this type of disorder.

Experimental data and computer modeling proved, that using well known multilayers that can easily be constructed with well established material science methods, more complex structures can be made which can be seen from a wide viewing area. The disorder (in-plane, out-plane), the properties of the multilayer (layer thicknesses and refractive indexes) provide several possibilities of further experiments to fine-tune the optical properties.

## Acknowledgments

The work in Hungary was supported by OTKA grant PD83483.

## 7. References

1. J. D. Joannopoulos, R. D. Meade, and J. N. Winn, *Photonic Crystals: Molding the Flow of Light*, Princeton University Press, Princeton, 2nd edition (2008).

2. I. El-Kady, M. M. Sigalas, R. Biswas, K. M. Ho, and C. M. Soukoulis, “Metallic photonic crystals at optical wavelengths,” *Phys. Rev. B* **62**(23), 15299-15302 (2000).

3. K. Kertész, Zs. Bálint, Z. Vértesy, G. I. Márk, V. Lousse, J.-P. Vigneron, M. Rassart, and L. P. Biró, “Gleaming and dull surface textures from photonic-crystal-type nanostructures in the butterfly *Cyanophrys remus*,” *Phys. Rev. E* **74**, 021922 (2006).

4. K. Kertész et. al., “Photonic band gap materials in butterfly scales: A possible source of “blueprints”,” *Mater. Sci. Eng. B* **149**, 259-265 (2008).

5. L. P. Biró, K. Kertész, Z. Vértesy, G. I. Márk, Zs. Bálint, V. Lousse, and J.-P. Vigneron, “Living photonic crystals: Butterfly scales — Nanostructure and optical properties,” *Mater. Sci. Eng. C* **27**, 941-946 (2007).

6. K. Edagawa, S. Kanoko, and M. Notomi, “Photonic Amorphous Diamond Structure with a 3D Photonic Band Gap,” *Phys. Rev. Lett.* **100**, 013901 (2008).

7. P. D. García, R. Sapienza, Á. Blanco, and C. López, “Photonic Glass: A Novel Random Material for Light,” *Adv. Mater.* **19**, 2597-2602 (2007).

8. D. R. Smith, J. B. Pendry, and M. C. K. Wiltshire, “Metamaterials and Negative Refractive Index,” *Science* **305**, 788-792 (2004).

9. K. Busch, G. von Freymann, S. Linden, S. F. Mingaleev, L. Tkeshelashvili, and M. Wegener, “Periodic nanostructures for photonics,” *Phys. Rep.* **444**, 101-202 (2007).

10. S. Kinoshita, *Structural Color in the Realm of Nature*, World Scientific, Singapore (2008).

11. L. P. Biró, and J.-P. Vigneron, “Photonic nanoarchitectures in butterflies and beetles: valuable sources for bioinspiration,” *Laser Photon. Rev.* **5**(1), 27-51 (2011).

12. G. I. Márk, Z. Vértesy, K. Kertész, Zs. Bálint, and L. P. Biró, “Order-disorder effects in structure and color relation of photonic-crystal-type nanostructures in butterfly wing scales,” *Phys. Rev. E* **80**, 051903 (2009).

13. Zs. Bálint, K. Kertész, G. Piszter, Z. Vértesy, and L. P. Biró, “The well-tuned blues: the role of structural colours as optical signals in the species recognition of a local butterfly fauna (Lepidoptera: Lycaenidae: Polyommatinae),” *J. R. Soc. Interface* **9**(73), 1745-1756 (2012).

14. J. Haberko, and F. Scheffold, ”Fabrication of mesoscale polymeric templates for three-dimensional disordered photonic materials,” *Opt. Express* **21**(1), 1057-1065 (2013).

15. K. Chung et. al., ”Angle-Independent Reflectors: Flexible, Angle-Independent, Structural Color Reflectors Inspired by Morpho Butterfly Wings,” *Adv. Mater.* **24**(18), 2366 (2012).

16. T.-H. Chang et. al., ”Fabrication of three-dimensional photonic crystals using autocloning layers on the self-assembled microspheres,” *Optic. Engin.* **48**(7), 073401 (2009).

17. Gy. Tolnai, F. Csempesz, M. Kabai-Faix, E. Kálmán, Zs. Keresztes, A. L. Kovács, J. J. Ramsden, and Z. Hórvölgyi, ”Preparation and Characterization of Surface-Modified Silica-Nanoparticles,” *Langmuir* **17**(19), 2683-2687 (2001).

18. P. Kozma, B. Fodor, A. Deák, and P. Petrik, “Optical Models for the Characterization of Silica Nanosphere Monolayers Prepared by the Langmuir-Blodgett Method Using Ellipsometry in the Quasistatic Regime,” *Langmuir* **26**(20), 16122-16128 (2010).

19. M. Leskelä, and M. Ritala, “Atomic layer deposition (ALD): from precursors to thin film structures,” Thin Solid Films 409, 138-146 (2002).

20. S. M. George, “Atomic Layer Deposition: An Overview,” *Chem. Rev.* **110**, 111-131 (2010).

21. A. F. Oskooi, D. Roundy, M. Ibanescu, P. Bermel, J. D. Joannopoulos, and S. G. Johnson, “Meep: A flexible free-software package for electromagnetic simulations by the FDTD method,” *Comput. Phys. Commun.* **181**(3) 687-702 (2010).

22. R. O. Prum, and R. H. Torres “A Fourier tool for the analysis of coherent light scattering by bio-optical nanostructures,” *Integr. Comp. Biol.* **43**(4), 591–602 (2003).

23. A. E. Seago, P. Brady, J.-P. Vigneron, and T. D. Schultz, “Gold bugs and beyond: a review of iridescence and structural colour mechanisms in beetles (Coleoptera),” J. R. Soc. Interface 6, S165-S184 (2009).

## Figure and table captions

**Figure 1.** Cross sectional geometry of the 3D FDTD model. The position of the source plane and the detector planes ($F_{layer}$ and $F_{refl}$) were also shown. The position of the $F_{layer}$ was varied in the different calculations to investigate the propagating mode in the multilayer. The materials that are used: gray – silicon substrate; blue – $SiO_2$; green – $TiO_2$

**Figure 2.** AFM (a, b, d) images of the layers of silica nanospheres with two diameters: (a-b): 156 nm, (d): 292 nm. (c) Fast Fourier transformed AFM image on the sample with smaller spheres, three of the ordered lattice directions are labeled by arrows. (e) The calculated radial average of the power spectrum on the sample with larger spheres. (f) Fourier transformed AFM image on the sample with larger spheres, the lack of long range order can be seen.

**Figure 3.** SEM images of the samples after $TiO_2/SiO_2$ multilayer deposition with (a) smaller spheres, (b) larger spheres and (c) a multilayer reference with 324 nm thermal oxide layer on silicon substrate. The cross section of the structures and the roughness of the surface of the samples can be seen.

**Figure 4.** Specular reflection of the samples with spheres, and a flat sample with thermal oxide layer below the multilayer. The illumination and detection were perpendicular to the sample surface.

**Figure 5.** Diffuse reflection of the samples: a) smaller, 156 nm spheres and b) larger, 292 nm spheres with multilayer on top. The illumination was perpendicular to the sample surface. High reflection can be seen under every detection angles around the wavelength range of 400-500 nm on both figures, but the angle dependence on the sample with larger spheres is much smaller. c – f) Photo of the samples with the same illumination setup (perpendicular to the sample surface). The samples from left to right: nanoarchitectures with 156 nm spheres, nanoarchitectures with 292 nm spheres, multilayer reference sample with 324 nm oxide. The angle of observation is c) 10°; d) 30°; e) 45°; f) 60°. Note that in agreement with the data in (a) the nanoarchitecture with 156 nm spheres changes color with the increasing of the viewing angle, while the color of the nanoarchitecture with the 292 nm spheres - in agreement with (b) - is essentially constant under all viewing angles. The flat multilayer does not exhibit any color when viewed under oblique angles.

**Figure 6.** Calculated specular reflection of the samples with 1D model, and 3D FDTD models. Samples with a) smaller spheres and b) larger spheres.

**Figure 7.** Time evolution ($t_1 < t_2 < t_3$) of the electric field perpendicular to the cross section ($E_y$) and the horizontal Pointing vector ($S_x$) with a wavelength around 435 nm, where the diffuse peak was found. The nanoarchitecture was built of the larger 292 nm spheres. The propagating mode in the $S_x$ images and the out scattering of light in the $E_y$ images can be seen. The blue colours are negative; the red ones are positive values.

**Figure 8.** Average diffuse reflectance of the samples with respect to a white diffuse standard ($R_{measured}$), compared to the calculated values by FDTD model ($F_{calculated}$).

**Figure 9.** Intensity of the propagating light within the multilayer in the samples with larger spheres. The distances, given in the upper right corner, were measured from the plane in the

multilayer below the center of the source. The reflection maximum decreased to 50 % at about 2500 nm distance from the source.

**Figure 10.** 3D FDTD calculations were done on smaller spheres (156 nm diameter) with modified geometries, where a sphere was raised above the sphere layer. The cross-section of the geometries can be seen on the right side, the blue area represents the regions below the radiation source plane. By the small modification, a significant increase by 5 to 10 times can be observed in the wavelength range of 350-550 nm.

**Table 1.** Refractive indexes and spectral ranges that were used in the refined 3D FDTD model

Figure1

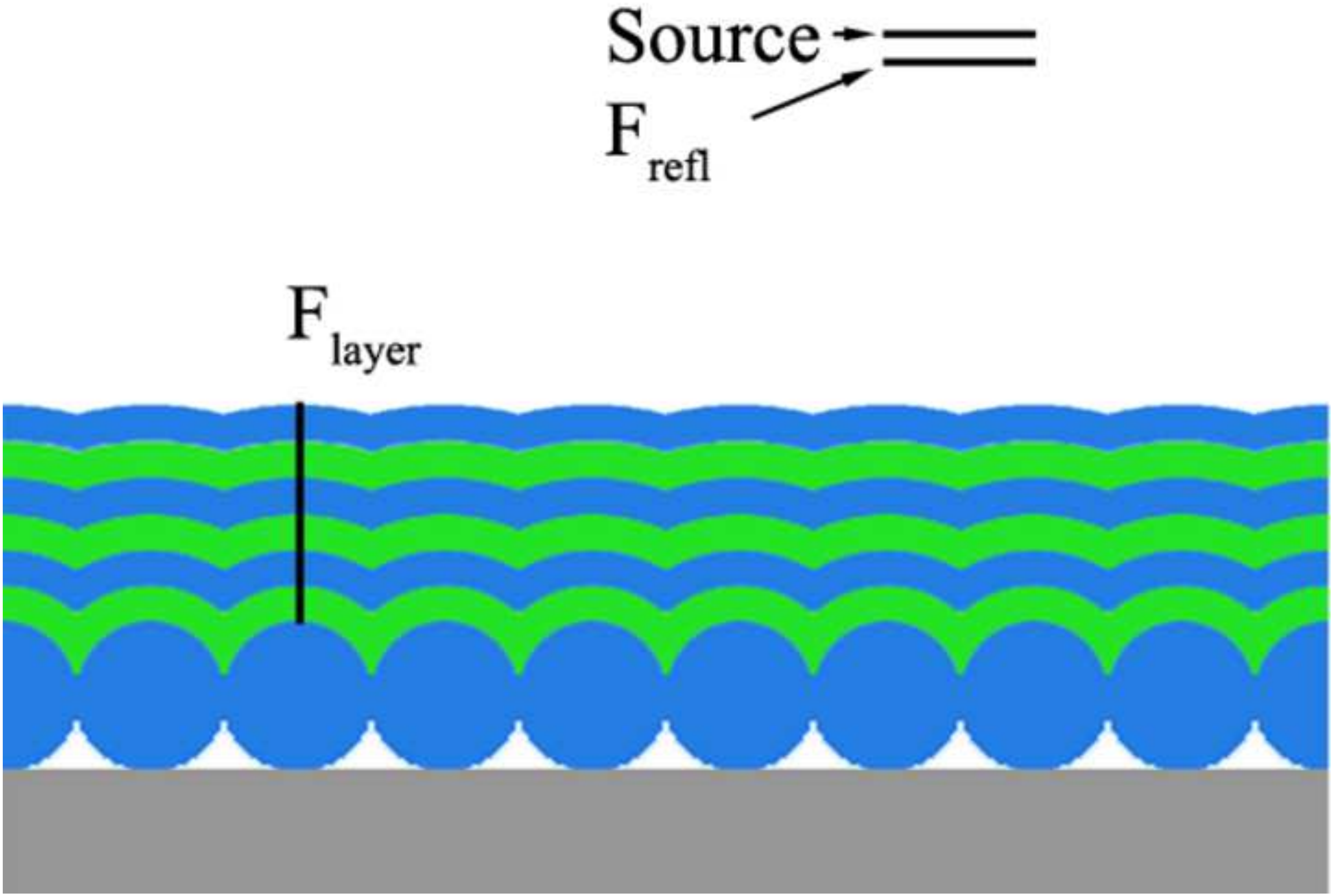

Figure2

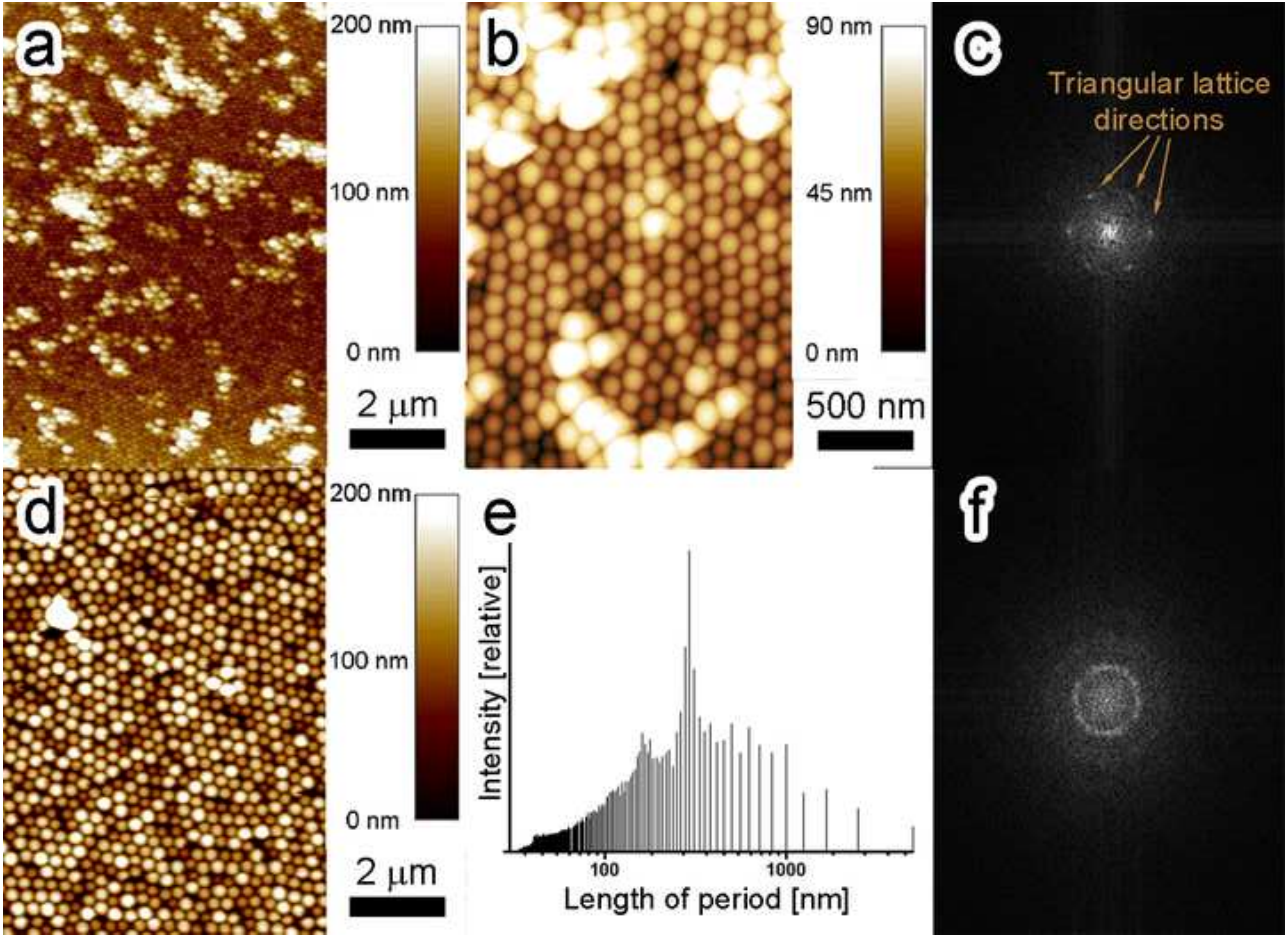
a
200 nm
100 nm
0 nm
2 µm
b
90 nm
45 nm
0 nm
500 nm
c
Triangular lattice directions
d
200 nm
100 nm
0 nm
2 µm
e
Intensity [relative]
100
1000
Length of period [nm]
f

Figure3

Click here to download high resolution image

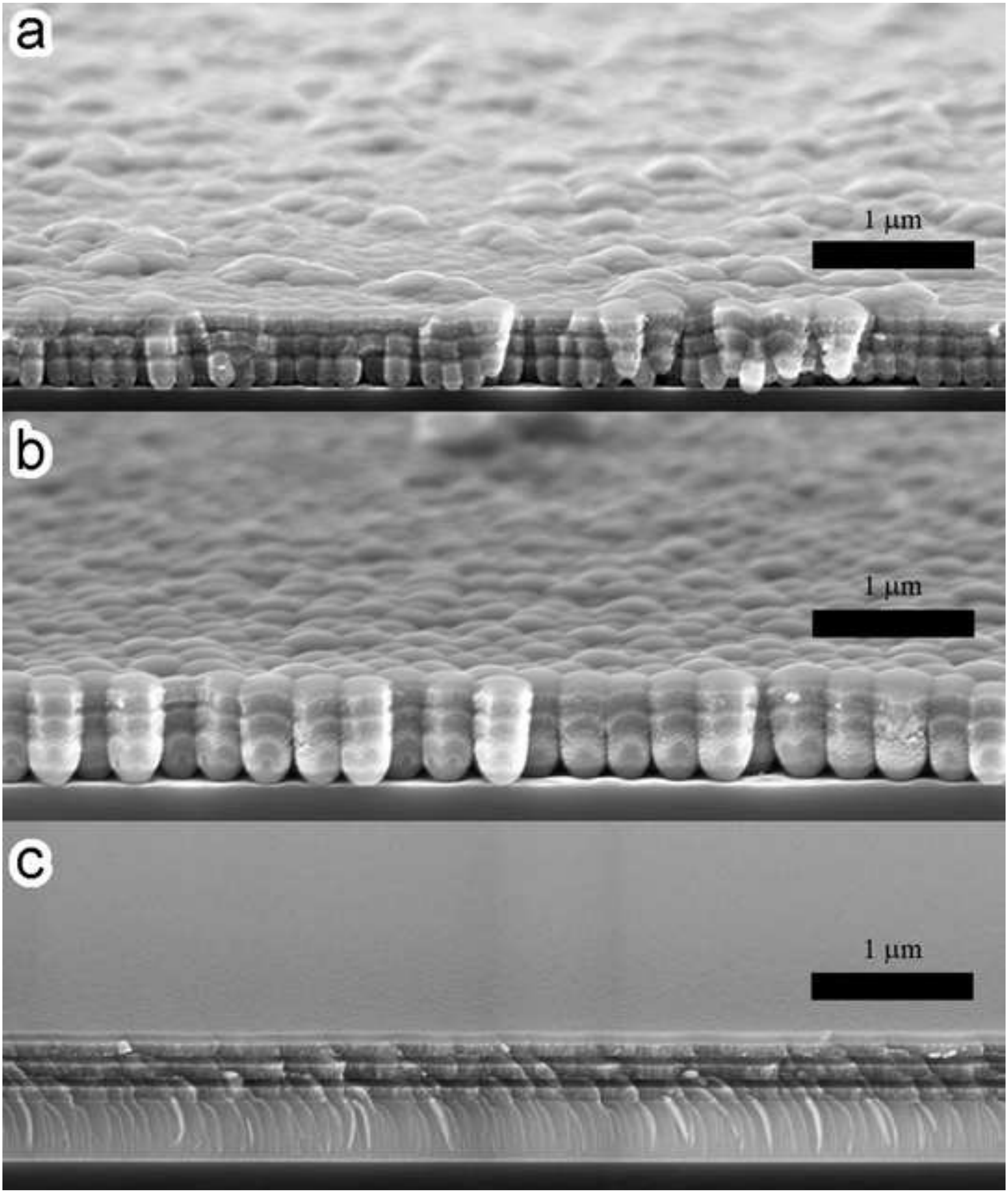

Figure4

Click here to download high resolution image

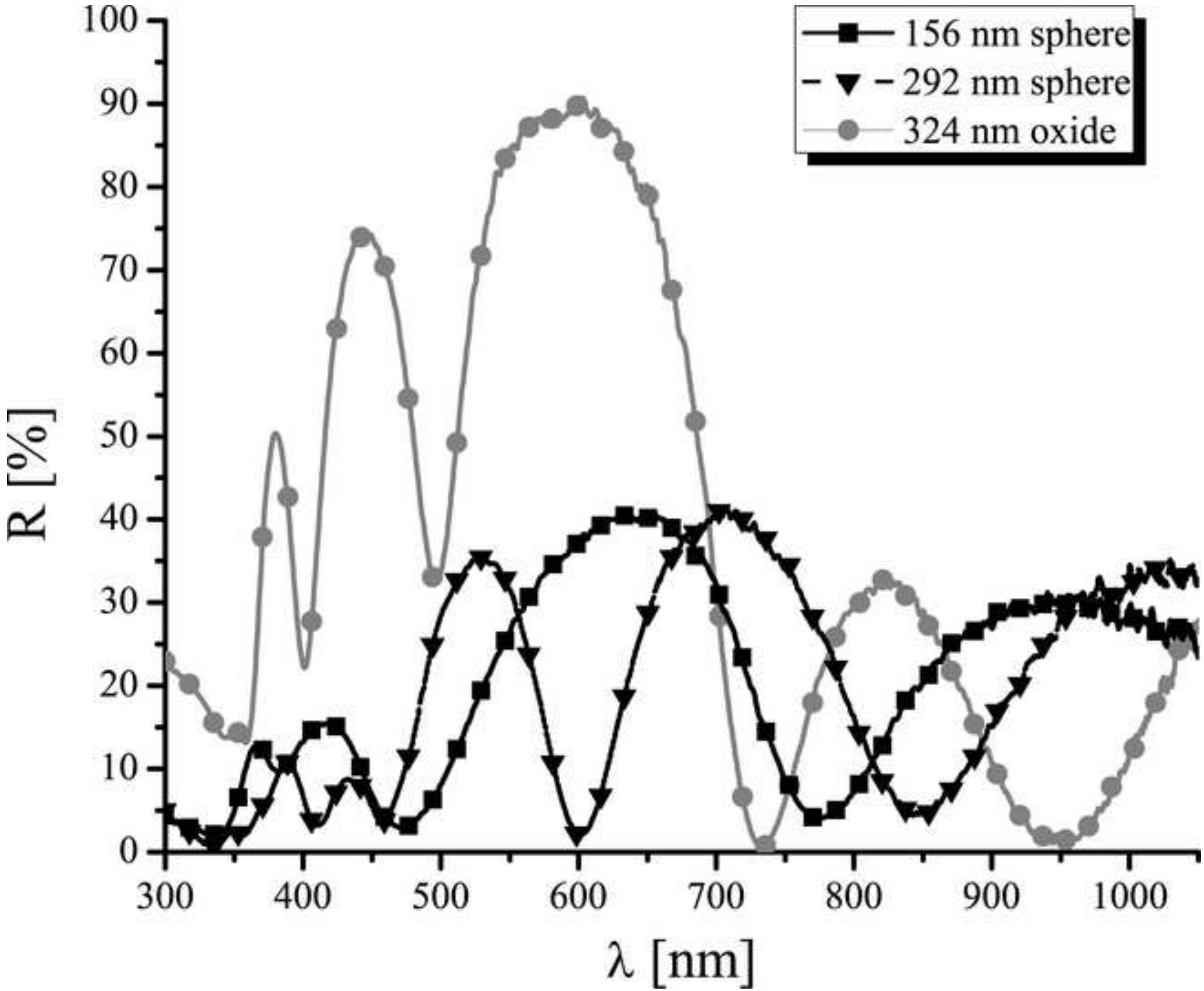

Figure5

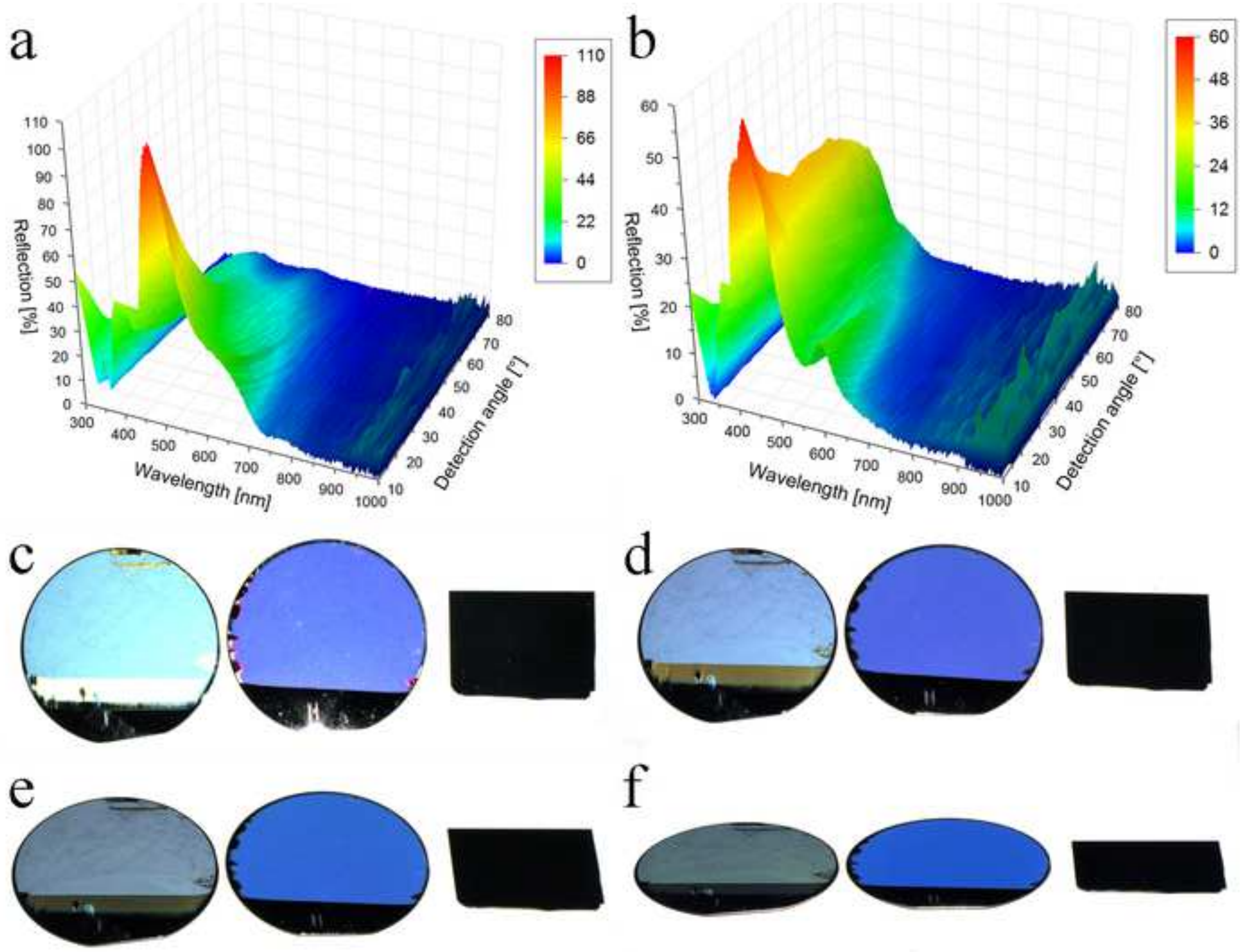
a
110
88
66
44
22
0
Reflection [%]
110
100
90
80
70
60
50
40
30
20
10
0
Wavelength [nm]
300
400
500
600
700
800
900
1000
Detection angle [°]
10
20
30
40
50
60
70
80
b
60
48
36
24
12
0
Reflection [%]
60
50
40
30
20
10
0
Wavelength [nm]
300
400
500
600
700
800
900
1000
Detection angle [°]
10
20
30
40
50
60
70
80
c
d
e
f

Figure6

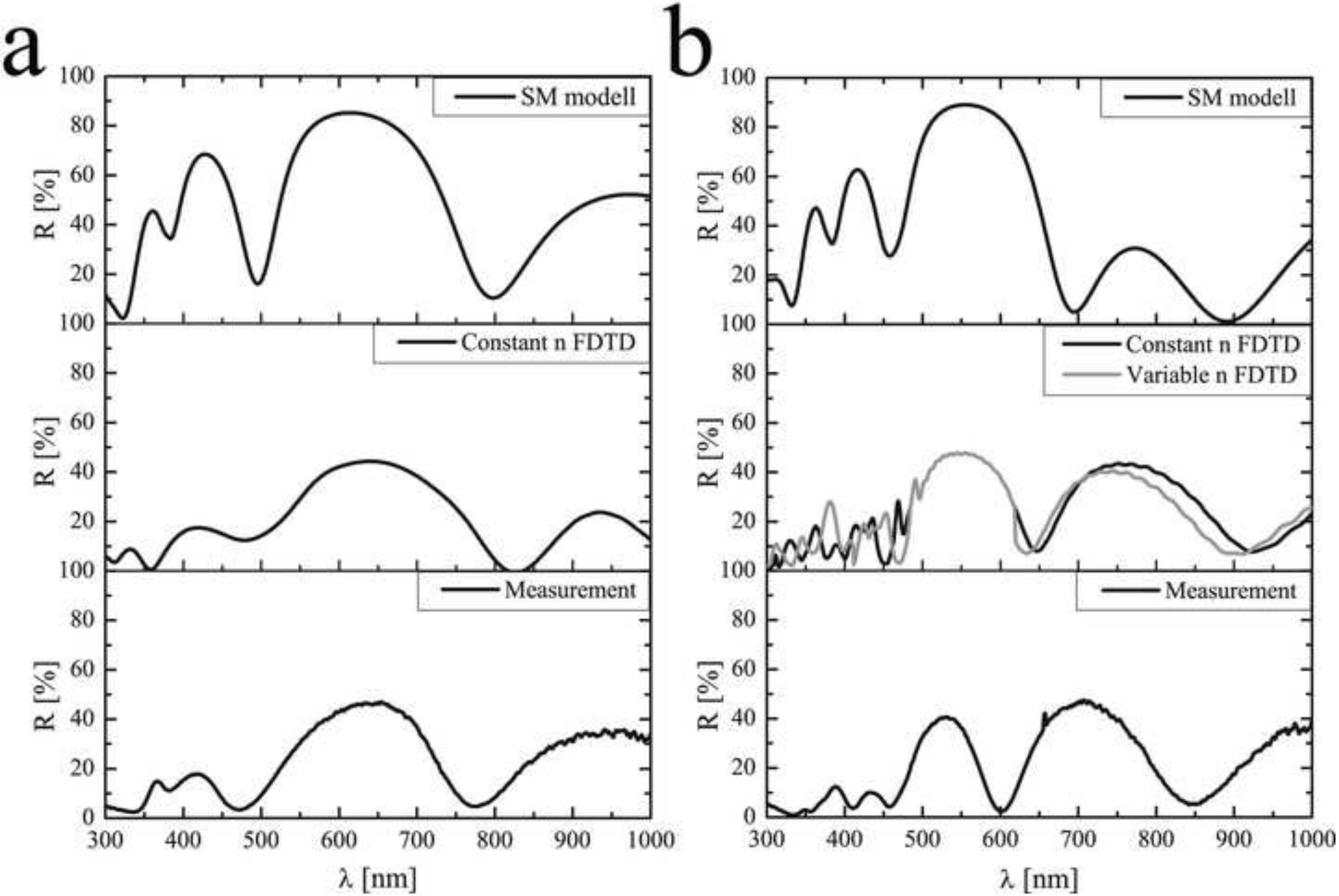
a
b
SM modell
Constant n FDTD
Variable n FDTD
Measurement
R [%]
0
20
40
60
80
100
300
400
500
600
700
800
900
1000
λ [nm]

Figure7

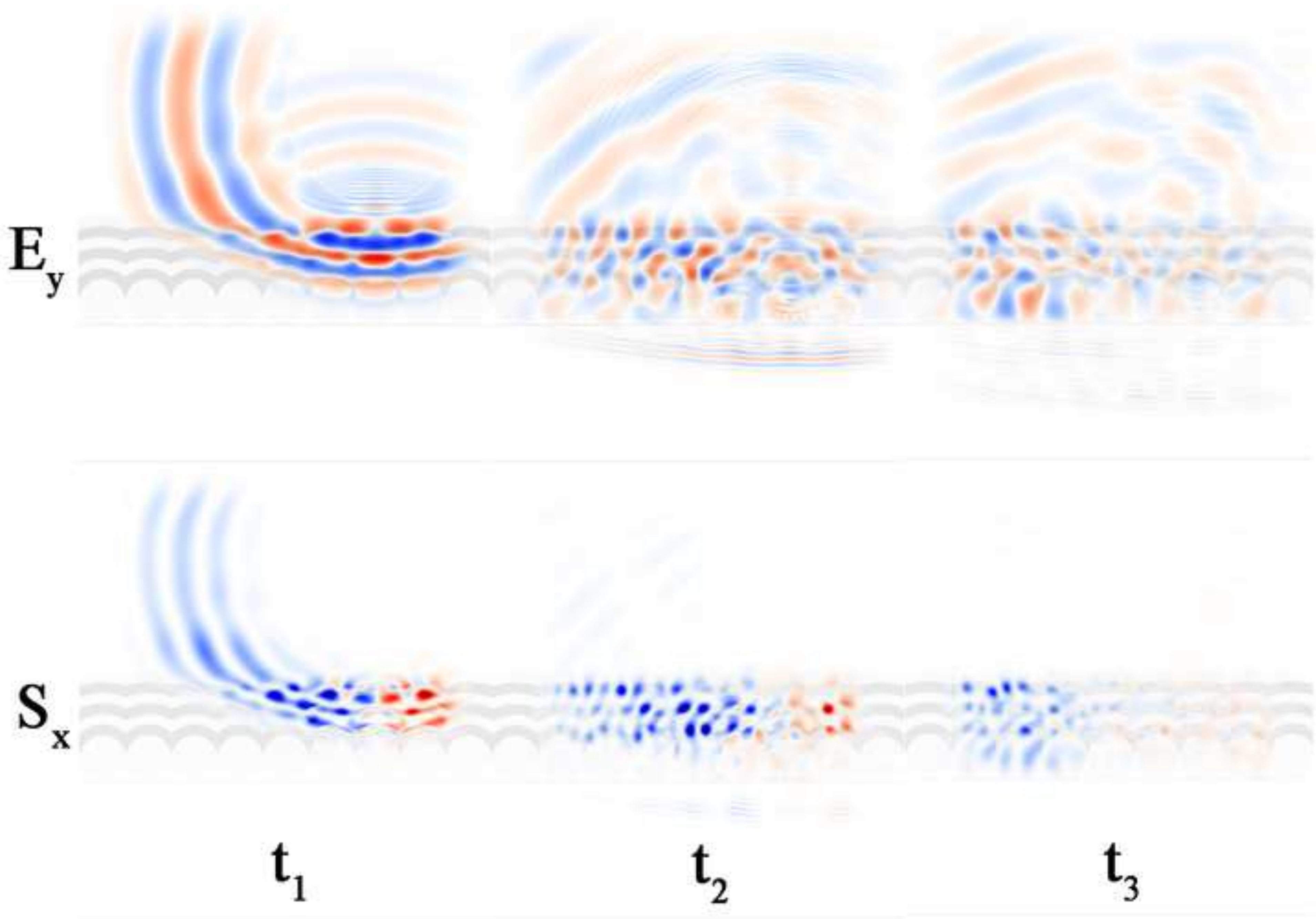

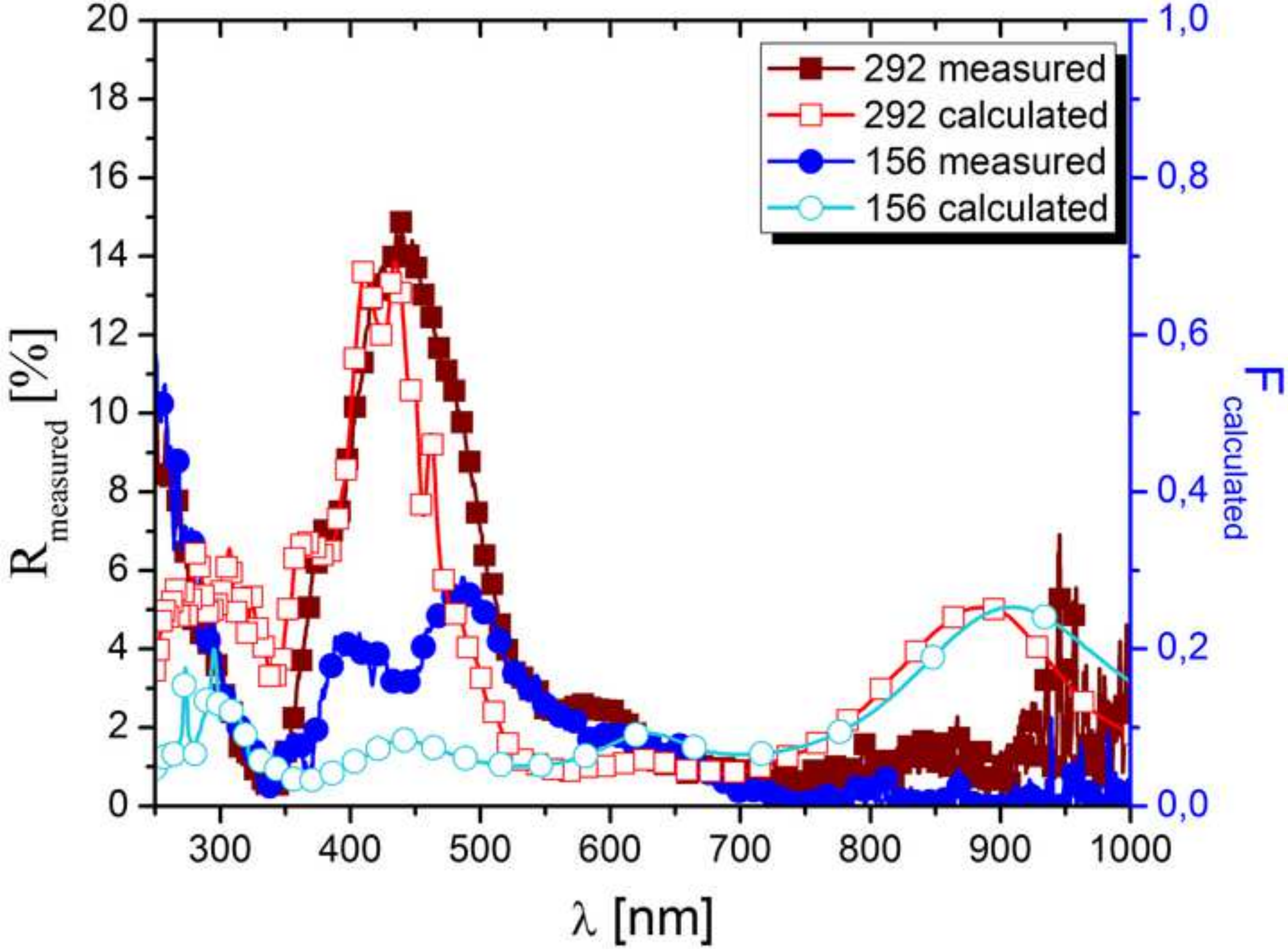

292 measured
292 calculated
156 measured
156 calculated
$R_{measured}$ [%]
$F_{calculated}$
λ [nm]
0
2
4
6
8
10
12
14
16
18
20
0,0
0,2
0,4
0,6
0,8
1,0
300
400
500
600
700
800
900
1000

Figure9

Click here to download high resolution image

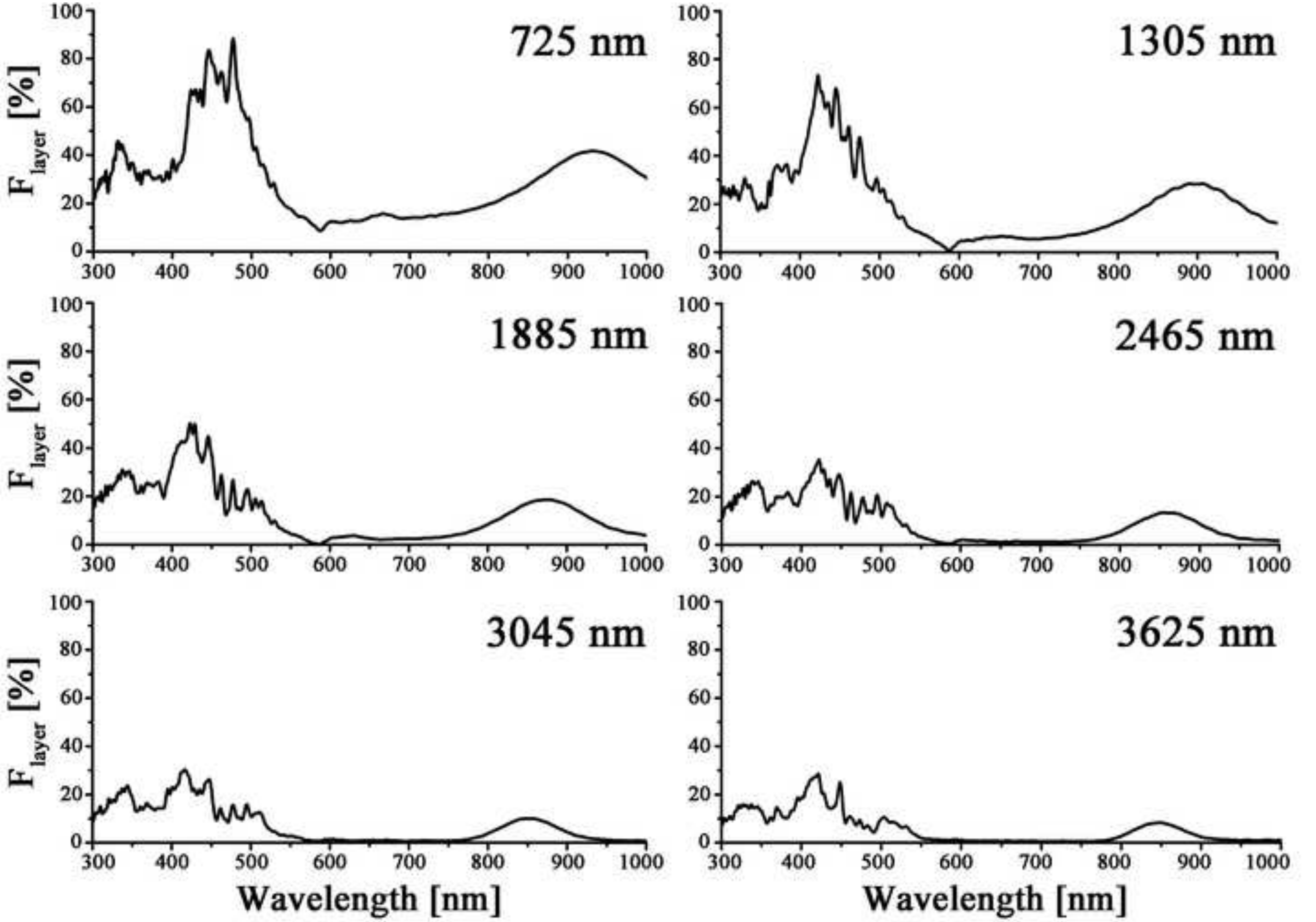

Figure10

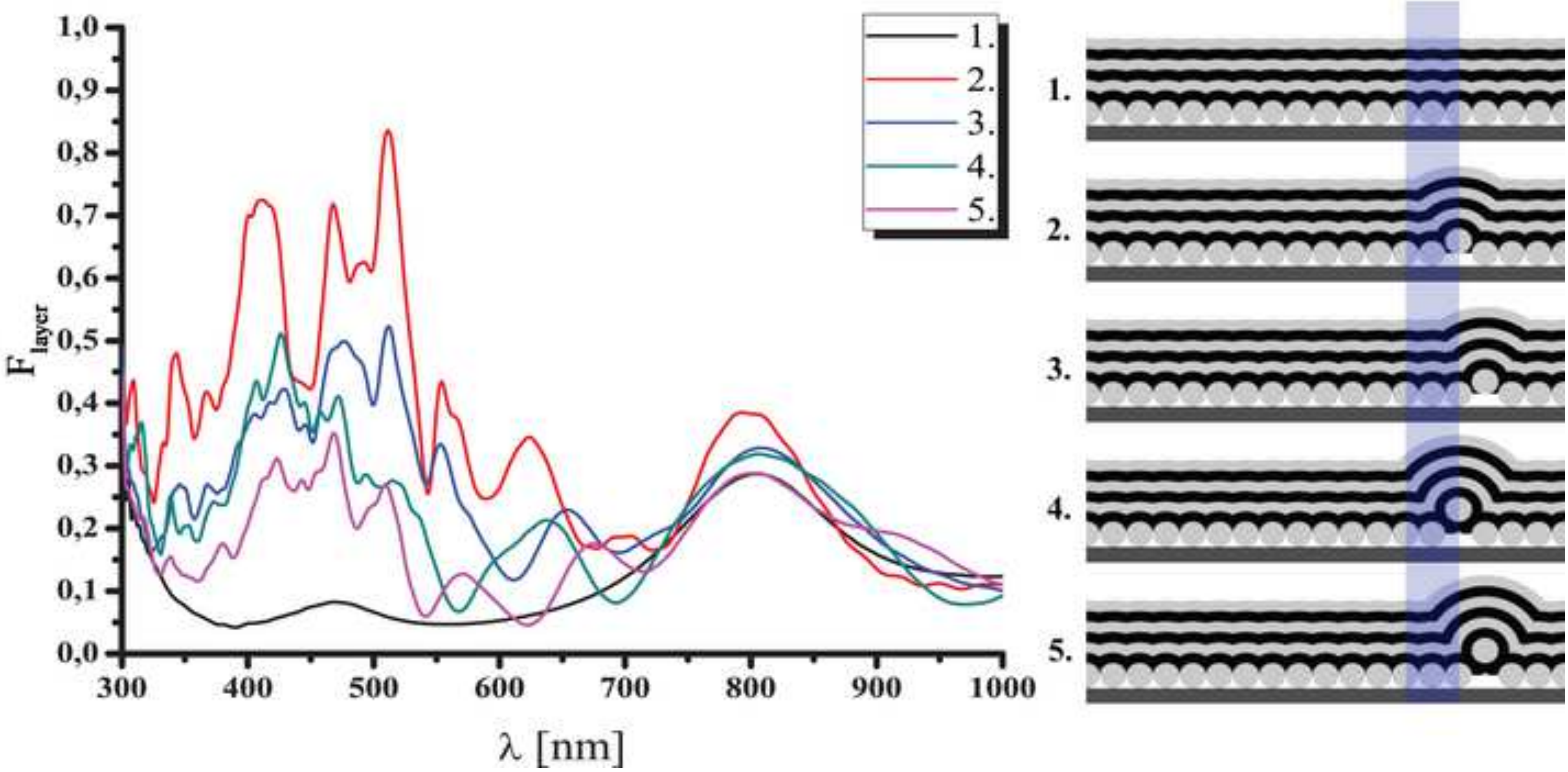
1,0
0,9
0,8
0,7
0,6
0,5
0,4
0,3
0,2
0,1
0,0
$F_{layer}$
300
400
500
600
700
800
900
1000
λ [nm]
1.
2.
3.
4.
5.
1.
2.
3.
4.
5.

Table1

| Spectral range | Refractive indexes | | | |
|---|---|---|---|---|
| | Wavelength | Si | SiO2 | TiO2 |
| 300-410 | 388 | 6 | 1.47 | 2.64 |
| 410-480 | 435 | 4.85 | 1.47 | 2.55 |
| 480-620 | 531 | 4.16 | 1.46 | 2.44 |
| 620-1000 | 708 | 3.77 | 1.45 | 2.35 |